

PCCP

Accepted Manuscript



This is an *Accepted Manuscript*, which has been through the Royal Society of Chemistry peer review process and has been accepted for publication.

Accepted Manuscripts are published online shortly after acceptance, before technical editing, formatting and proof reading. Using this free service, authors can make their results available to the community, in citable form, before we publish the edited article. We will replace this *Accepted Manuscript* with the edited and formatted *Advance Article* as soon as it is available.

You can find more information about *Accepted Manuscripts* in the [Information for Authors](#).

Please note that technical editing may introduce minor changes to the text and/or graphics, which may alter content. The journal's standard [Terms & Conditions](#) and the [Ethical guidelines](#) still apply. In no event shall the Royal Society of Chemistry be held responsible for any errors or omissions in this *Accepted Manuscript* or any consequences arising from the use of any information it contains.

Investigating Molecular Interactions and Surface Morphology of Wax-Doped Asphaltenes

Farideh Pahlavan^a, Masoumeh Mousavi^b, Albert Hung^c, and Ellie H. Fini^d (contact author)

a) Farideh Pahlavan, Ph.D.

Research Associate
Center for Innovation in Materials, Methods and Management
North Carolina A&T State University
1601 E. Market St, Greensboro, North Carolina, 27405
E-mail: farideh.pahlavan64@gmail.com
Tel: 98-71-36137165 Fax: 98-71-32286008

b) Masoumeh Mousavi, Ph.D.

Research Associate,
Center for Innovation in Materials, Methods and Management
North Carolina A&T State University
1601 E. Market St, Greensboro, North Carolina, 27405
E-mail: fereshteh_mou@yahoo.ca
Tel: 98-71-36137165 Fax: 98-71-32286008

c) Albert Hung, Ph.D.

Department of Nanoengineering
Joint School of Nanoscience and Nanoengineering, North Carolina A&T State University,
Greensboro, NC 27401
Email: ahung@ncat.edu
Office phone: 336-285-3676

d) Ellie H. Fini, Ph.D., P.E., Corresponding Author

Associate Professor of Civil Engineering
North Carolina A&T State University
1601 E. Market St, Greensboro, North Carolina, 27405
Email: efini@ncat.edu
Office phone: 336-285-3676

ABSTRACT

The nature and origin of bee-like microstructures (bees) in asphalt binders and their impact on asphalt oxidation have been the subject of extensive discussions in recent years. While several studies refer to the bees as solely surface features, some others consider them to be bulk microcrystalline components that are formed due to co-precipitation of wax and asphaltene molecules. In this study, we use a rigorous theoretical and experimental approach to investigate the interplay of asphalt components (mainly asphaltene and wax) and their impact on bee formation. In the theoretical section, quantum-mechanical calculations using density functional theory (DFT) are used to evaluate the strength of interactions between asphaltene unit sheets in the presence and absence of a wax component, as well as the mutual interactions between asphaltene molecules (monomers and dimers) and paraffin wax. The results of this section reveal that paraffin waxes not only do not reinforce the interaction between the asphaltene unit sheets, they destabilize asphaltene assembly and dimerization. AIM (Atom in Molecules) analysis shows the destabilizing effect of wax on asphaltene assembly as a reduction in the number of cage and bond critical points between asphaltenes. This destabilization effect among interacting systems (asphaltene-asphaltene and wax-asphaltene) does not support the hypothesis that interaction between paraffin waxes and non-wax components, such as asphaltene, is responsible for their co-precipitation and bee formation. To further examine the effect of wax component on asphalt microstructure experimentally, we used atomic force microscopy (AFM) to study the surface morphology of an asphalt sample doped with 1% to 25% paraffin wax. In agreement with the conclusions drawn from the DFT approach, our experiments indicate that paraffin wax tends to crystallize separately and form lamellar paraffin wax crystal inclusions with 10 nm thickness. Moreover, the addition of 3% wax into asphalt results in a significant increase in surface roughness from 0.5 nm to 4.1 nm and an increase in bee wavelength from 651 nm to 1038 nm.

Keywords: asphaltene dimer, bee structure, paraffin wax, bonding energy, density functional theory

INTRODUCTION

Petroleum-based asphalt is a by-product of petroleum refining. Asphalt binder or “bitumen” is one of the most commonly used paving materials, with a world market size of over \$100 billion. Approximately 94% of the four million miles of roadways in the United States have been paved with asphalt pavements, demanding continuous maintenance and rehabilitation that requires roughly eight billion gallons of liquid asphalt (costing \$19 billion) per year.¹⁻³ Added to that are the consumption of liquid asphalt to pave parking lots and driveways, seal cracks, stabilize the subgrade and base, and make roofing shingles.

Accordingly, there have been several studies focusing on the characterization of asphalt binder at the molecular level, in an attempt to not only predict its performance more accurately but also enhance its properties and service life. Asphalt binders are commonly categorized by their solubility in organic solvents into four groups called SARA: saturates, aromatics (naphthene aromatics), resins (polar aromatics), and asphaltenes. Interactions among the aforementioned constituents are known to be responsible for much of the structuring (intermolecular associations) that has a significant influence on the physical properties and behavior of asphalt.⁴⁻⁷ Among many structuring features of asphalt binder,^{8,9} “bee-like structures” have recently received attention from several researchers trying to determine their origin and nature as well as their evolution due to environmental conditions.

Bee structures, whose name came from their apparent resemblance to a bumble-bee with yellow and black stripes, were first reported by Loeberet et al.¹⁰ in their study of bitumen microstructures using atomic force microscopy (AFM). These geometric features are, indeed, wavy interiors in an elliptical domain with a strong influence on the rheological properties of bitumen. AFM distinguishes three phases of bee structures (the distinctions between these phases will be clearer from pictures later in the paper): catana-phase (corresponding to the dispersed bee structures), peri-phase (surrounding catana-phase), and para-phase (a smooth matrix encompassing catana-phases and peri-phases in a larger domain).

Although a considerable number of investigations have been carried out on the origin of bitumen microstructures, there is still disagreement within the asphalt community about their origin.^{8, 11} Inspired by Loeber's observation that mainly reported bee structuring in bitumen with high asphaltene content,⁵ some researchers tried to find a correlation between asphaltene component and the extent and formation of bee structures. Based on AFM work on bitumen, this surface structuring was primarily attributed to asphaltene aggregation and the gel nature of asphalt.^{6, 8, 10, 12, 13} However, in recent years, the idea of wax crystallization in bitumen as the origin of bee phases has attracted particular attention. This idea has been supported by De Moraes,¹⁴ Schmets,¹⁵ Pauli,¹⁶ and others,^{17, 18} who argued that the interaction between crystallizing n-paraffin waxes and other non-polar fractions of asphalt binder is responsible for the formation of bee microstructures. Pauli¹⁶ supported his hypothesis by presenting evidence of significant structuring in non-polar fractions of an asphalt binder after removal of its polar aromatic fractions (asphaltenes and resins).¹⁶ On the other hand, the interaction of crystallizing n-paraffin waxes with polar components of asphalt has been the subject of other investigations.^{9, 19, 20} In these studies, flocculated asphaltenes are considered as nucleation sites for wax crystallization to form highly insoluble organic composites (made of long n-alkanes and highly aromatic asphaltenes), which contributes to the formation of bee-like structures.

Other researchers^{18, 21-23} also documented that, besides the wax contribution, factors such as the concentration of asphaltenes and oxidative aging are involved in the development of bee structures. In addition, some recent studies were devoted to bee mechanical fracture and topological evolution.²⁴ Other studies have established a relation between bee size and rheological properties of asphalt,^{25, 26} indicating bee length can have a moderating effect on the relationship between viscosity and stiffness²⁵ and that binders that have larger bees typically show higher stress amplification due to tensile deformation.²⁶ Although the impact of bees on asphalt properties has been shown, there is still disagreement about the nature and origin of bees, as well as their impact on asphalt aging.

In this paper, we use a rigorous theoretical approach and experimental observations to investigate favorable molecular interactions within an asphalt matrix (mainly asphaltene and wax) as a possible cause for bee formation. The theoretical analysis is based on a high quantum level of dispersion-corrected density functional (DFT-D) approach; the experimental analysis is based on atomic force microscopy (AFM). The main objectives in the theoretical section are evaluation of the nature and strength of interactions between asphaltene-asphaltene flakes as a function of the wax component, and also asphaltene-wax interactions. On the basis of DFT-D results, the promoting effect of wax crystals supports the idea of wax-asphaltene co-crystallization to form bee morphology, while the inhibiting effect of wax gives credence to the phase separation theory that indicates bees are mainly waxes. To examine in a laboratory setting the hypothesis derived from theoretical calculations, atomic force microscopy (AFM) is used to investigate the effects of wax on morphological characteristics of asphalt in a wax-doped asphalt complex.

METHODS AND MATERIALS

In this paper, theoretical calculations at the molecular level were carried out within the framework of the DFT-D level being embedded in the Gaussian 09 program.²⁷ It should be noted that the conventional DFT exchange-correlation functionals are not usually sufficient for providing a complete description of the long-range electron correlations responsible for dispersive forces in stacking systems.²⁸ This imperfection is corrected by adding an empirical London dispersion term into the Kohn-Sham total energy to treat the weak interaction between fragments.^{29, 30} The geometry optimization and electronic structure computations have been performed using the semi-empirical dispersion-corrected functional, B97-D. The mentioned GGA-type method is based on Becke's functional,³¹ which is extended to take into account a van der Waals (VDW) correction by including a damped $C_6 \cdot R^{-6}$ term.²⁹ The basis set for all atoms has a double- ξ quality augmented with one polarization function of 6-31G*. Binding energy (E_{bind}) for each aggregation has been calculated through Equation 1:

$$E_{bind} = E_{complex} - (E_{frag1} + E_{frag2}) \quad (1)$$

Where E_{frag1} and E_{frag2} are the total energies of the fragments and $E_{complex}$ is the total energy of the microstructure consisting of the two molecules. However, for the systems associated with geometrical restructuring, binding energy cannot be a good descriptor for characterization of interactions. The interaction energy is a statement of the strength of interactions and is suggested for systems with substantial reconstruction.³²⁻³⁶ So, interaction energy should be considered in addition to binding energy for microstructure association. Interaction energy is calculated by Equation 2:

$$E_{int} = E_{bind} - (\Delta E_{frag1} + \Delta E_{frag2}) \quad (2)$$

In this definition, ΔE_{frag1} and ΔE_{frag2} refer to the deformation energy of fragments, which is defined as the difference between the energy of the free molecule in gas-phase and the energy of the isolated and distorted molecule in complex. Negative E_{bind} and E_{int} values correspond to stable interactions. The basis set superposition errors (BSSE) were accounted for in all calculated energies at the B97-D/6-31G* level of theory by the counterpoise (CP) correction method.³⁷ In the CP procedure, the corrected energies of fragments in the full basis of the complex are applied to compute the interaction energy. In addition, quantum theory of atoms in molecules (QTAIM)³⁸ analysis was carried out on optimized structures to reveal the nature of interacting bonds. The electron density, $\rho(r)$, its Laplacian, $\nabla^2\rho(r)$, and the electronic energy density, $H(r)$, at critical points (CPs) were computed based on Bader's QTAIM using the AIM2000³⁹ program.

To further examine the results of calculation in a real laboratory setting and examine effects of wax on overall asphalt structures, morphological characteristics of asphalt in the presence of various percentages of paraffin wax were studied using atomic force microscopy (AFM). To do so, specimens were prepared on glass microscope slides that were cut into squares (0.5× 1 inches) and cleaned by ultrasonication in acetone followed by isopropanol and then water. Paraffin wax (P31, with melting point of 53-57 °C, acquired from Fisher Scientific) was added to PG 64-22 bitumen (acquired from Associated

Asphalt Inc.) in different weight percentages of 1% - 25% relative to the weight of the base bitumen. Physiochemical properties of the bitumen used in this study are shown in Table 1.

Table 1. Characteristics of the asphalt binder used in this study

Physical and Mechanical Properties	Specific Gravity @15.6 °C	1.039
	Flash Point, Cleveland Open Cup, °C	335
	Change in Mass RTFO	-0.0129
	Absolute Viscosity at 60 °C, Pa.s	202
	Stiffness (MPa) at -12°C @ 60s	112.5
	m-value at -12°C @ 60s	0.4
	Glass Transition Temperature (°C)	-14.55
	Complex modulus (Pa) @ 10rad/s; 64°C	1,544 pa
SARA Analysis	Saturates	9.2
	Aromatic	44.02
	Resin	39.92
	Asphaltene	6.84
Elemental Composition	C	81.6
	H	10.8
	N	0.77
	O	6.83

Samples of 15 – 30 mg were heated to 80 °C, stirred until thoroughly mixed, and cast onto a glass slide. It was observed that samples with high wax content were susceptible to separation if left undisturbed, so all samples were cast immediately after agitation at a molten stage. To prepare specimens for the fracture test, a second piece of glass was placed on top of each newly-cast bitumen sample. All samples were annealed in a convection oven at 150 °C for 40 min and allowed to cool and equilibrate under ambient conditions (22 °C, 50% humidity) for at least 24 hr. After annealing, the sandwiched bitumen was placed under compression to achieve a thin film [50 – 200 µm] thick. To fracture a sample, a

razor blade was wedged between the glass slides and used to lever them apart; caution was practiced to avoid fracturing the glass slides. Typically, the sample fractured in a brittle manner, characterized by a very sudden separation of the glass sandwich and a glossy, reflective bitumen surface (except for high-wax samples). On rare occasions, the sample would deform plastically, characterized by a gradual separation of the glass sandwich and a rough, non-reflective bitumen surface. AFM imaging focused on brittle fracture surfaces and was performed immediately with a 5600LS Atomic Force Microscope (Keysight Technologies) in tapping mode with TAP-300 silicon cantilever tips (Budget Sensors, 40 N/m nominal spring constant, 300 kHz nominal frequency). The amplitude set point was typically above 75% of the reference amplitude to reduce tip-sample pressure. Images were processed and analyzed with Gwyddion and ImageJ open-source software.

RESULTS AND DISCUSSION

The correlation between the formation of bee structures and the nature of interaction between asphaltene and wax molecules is studied through quantum-level analysis using DFT calculation as well as morphological study using the AFM method. To conduct DFT analysis, asphaltene flakes with and without the presence of wax components are examined at the molecular level. To this end, monomers and dimers of asphaltene are studied to determine the optimum conformation and relative geometry of two asphaltene monomers. After that, asphaltene molecules are optimized and then studied in the presence of wax monomers through a quantum-level DFT approach.

Asphaltene Monomer

Among the two most likely molecular structures of asphaltene (island and archipelago), the island model is believed to be the more predominant and stable one.⁴⁰⁻⁴² Asphaltene aggregates are mainly described through this model. The typical island model, used in this study, is a modified version of the Yen-Mullins

model,⁴³ newly proposed by Greenfield and Li,⁴⁴ which is more reflective of true asphaltene molecular structure. To alleviate the pentane effect⁴⁵ and corresponding high internal energy, the position of some aliphatic side chains is changed in modified Yen-Mullins structures.⁴⁴ Based on Mullins studies, this sulfur-based structure (called asphaltene-thiophene) can form asphaltene nanoaggregates with displaced stacks of PAH and with aggregation numbers of ~ 6 .⁴⁶

The complete and reduced forms of asphaltene-thiophene are shown in Figure 1. As the first step, the reduced form of an asphaltene-thiophene molecule (with no chains) is optimized and studied.

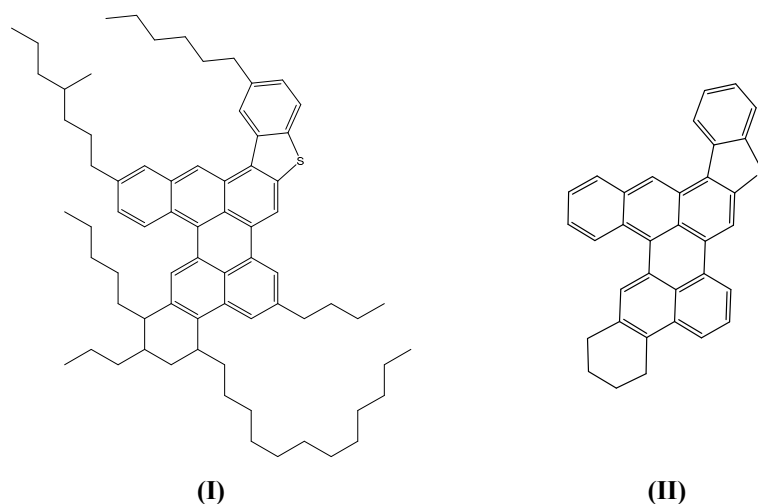


Figure 1. Structure of asphaltene-thiophene monomer (I) with side chains and (II) without side chains

The optimized structure, at the B97-D/6-31G* level, clearly shows the non-planarity of the aromatic core, which is in full accordance with recent reports about asphaltene-thiophene. This deviation from intermolecular planarity is attributed to the pentane effect and geometrical strain due to neighboring rings.^{44, 47, 48}

An electrostatic potential map of the reduced form of asphaltene is shown in Figure 2. Electrostatic models are sets of point charges that represent electrostatic charge distribution over the molecule. The relative distribution of charge can convey a variety of information such as polarity, electronegativity, nature of the bonds, and, most importantly, finding a proper way for having an effective

interaction. The color map, shown in Figure 2, has been generated at the B97-D/6-31G* level, with isosurfaces of 0.01 electrons au^{-3} , through GaussView package.⁴⁹ In this color spectrum, red represents the lowest (negative charge) and blue represents the highest (positive charge) electrostatic potential energy value. Our primary interest in this map is identification of the reactive sites of the molecule to design an effective interaction between two monomers of asphaltenes. Reactive sites of this sheet are charged regions that have a particular affinity for interacting with the second monomer. As shown in Figure 2, the negative charge has been localized at the center of the asphaltene sheet, and the positive charge is at the periphery. The localization of electron density around the sulfur atom describes this atom as an electron-rich center, verifying its higher electronegativity compared to nearby atoms.

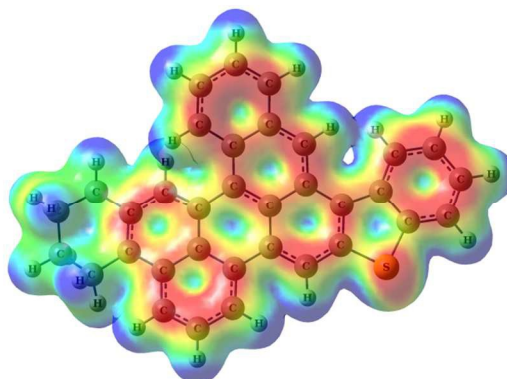


Figure 2-a. Electrostatic potential surface generated at the B97-D/6-31G* level, scaled between -0.6 (red) to 37.7 (blue) kcal/mol, with red and blue colors signifying regions with charge accumulation and depletion, respectively

Asphaltene Dimer

Self-association of the asphaltene sheets is considered as the first step in the formation of precipitated asphaltene particles. Therefore, designing the asphaltene dimer is considered as the first challenge. The suggested conformations for the association of two asphaltene monomers are based on the variation of the relative angle between two asphaltene sheets. The presence of heteroatoms and side chains increases the variety of conformations as starting structures for calculations. Three commonly used conformations are schematically shown in Figure 2-b: parallel (face-to-face), displaced-parallel (offset), and T-shape.

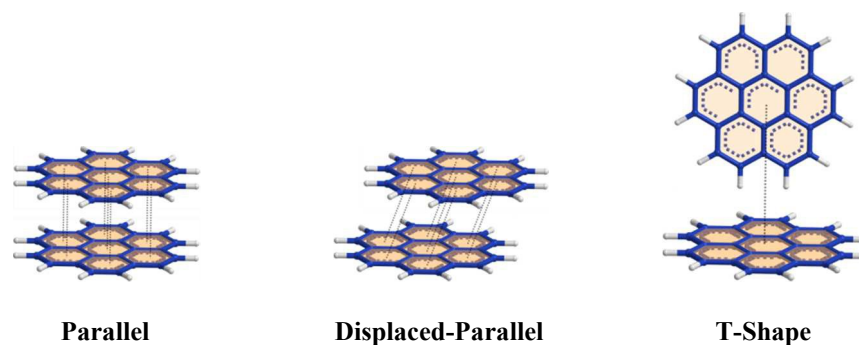


Figure 2-b. Representative models of polycyclic aromatic hydrocarbon (PAH) stacking systems

Although dimerization of benzene molecules does not follow the same behavior as asphaltene dimers, the association behavior of benzene molecules, as the building blocks of asphaltene monomers, has always been the center of attention. In this respect, the T-shape structure, with the minimum repulsive interactions, is the preferred structure of a benzene dimer.⁵⁰⁻⁵³ In the case of coronene, comprised of six benzene rings, the perpendicular arrangement is still the preferred arrangement for two neighboring molecules.⁵⁴

Based on available reports, the behavior of asphaltene aggregation is somehow different. Pacheco-Sánchez et al. reported that asphaltene orientations and morphology of the aggregates mostly depend on the asphaltene characteristics, corresponding to the various molecular structures.⁵⁵ Their molecular dynamic calculations on four asphalt models (Mullins, Speight, Zajac, and Murgich) led to the suggestion of three highly probable orientations of asphaltene aggregates: parallel, displaced-parallel (offset), and T-shape.⁵⁵ While Pacheco-Sánchez et al. theoretically verified the role of increasing temperature on decreasing the size of aggregation,⁵⁶ Greenfield and Zhang further documented that this factor could even alter the orientation of asphaltene monomers, leading to a change in aggregate formation.⁴⁷ The aromatic nature of the core and the distance between sheets are other factors affecting the arrangements of asphaltene sheets.⁴⁷

Regardless of temperature and its probable role in molecular orientation, offset π -stacking has been reported as the most efficient form for two interacting asphaltene monomers. The low tendency of

the system towards packing in a T-shape is mostly attributed to the steric hindrance of aliphatic chains.^{55, 57, 58}

To further examine asphaltene orientation, we investigated all possible modes of stacked asphaltene dimers, focusing on the position of sulfur atoms. No particular constraints were imposed over optimization processing. In the gas phase and at this level of calculations, all structures starting in a T-shape were optimized to the parallel configurations, and no stable structure in a T-shape was identified. This observation and the general consensus on π - π stacked geometries as the most efficient interacting geometries motivated us to focus on this orientation to pursue our main goals.

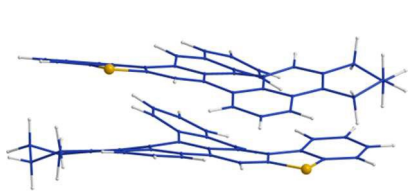
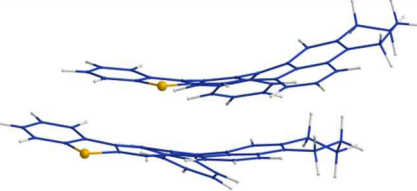
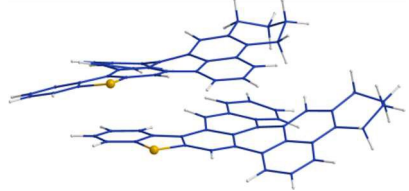
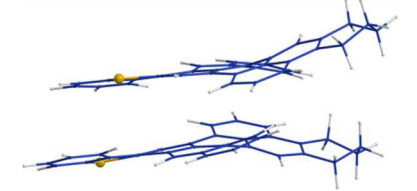
Table 2 shows the four lowest-energy structures (denoted D1-D4) differing in the relative orientation of the sulfur heteroatom. This table reports the optimum distance between two mass centers of asphaltene sheets (d), the relative energy of each dimer (ΔE_{tot}) defined with respect to the total energy of the lowest energy state (D1), the binding energy (E_{bind}) as the thermodynamic stability of the system, and the interaction energy (E_{int}) as a function of the strength of interactions.

Dimers D1 and D2 are the two most stable configurations; they are isoenergetic and π -stacked in offset style. An offset stack is a favorable arrangement at which π -electron repulsion of quadrupole/quadrupole interactions between the sheets is minimized, and the dimer becomes stabilized. At this level of calculations, the binding energy for each of these two most stable structures is about 28 kcal/mol. As expected, deformation of the fragments (asphaltene monomers) and their corresponding energies is not high (1.7 and 2.3 kcal/mol), and no significant difference is observed between interaction energy and binding energy.

In the D3 structure, an offset π -stacked arrangement is still preserved, while the asphaltene sheets are located in the maximum distance (5.407 Å) with respect to each other. This relatively large distance reduces the interaction between the sheets, which is reflected in the relatively lower binding and interaction energy values reported in Table 2.

In the D4 structure, the distance between the centers of the asphaltene sheets is shorter compared to D3, but D4 is the most unstable conformer. The reason behind this lower stability is the parallel arrangement of asphaltene sheets and the consequent strong repulsion of the electron clouds between the two sheets. These negative effects become less pronounced in the presence of a sulfur atom. Such behavior is rationalized through the Hunter-Sanders rule,^{59, 60} which presumes that electron-withdrawing substituents or heteroatoms decrease the negative charge of the ring π -electrons and provide a favorable electrostatic stabilization of the complex. The electron-rich region around a sulfur center, shown in Figure 2-a, is indicative of the electron-withdrawing character of a sulfur atom. This atom pulls electron density away from the center of fused rings, decreasing the negative charge of the π -electron cloud and subsequently enhancing the interaction between two parallel asphaltene sheets.

Table 2. Optimized asphaltene dimers, with all reported energies counterpoise corrected and in kcal/mol: optimum distance (d in Å) between two centers of asphaltene sheets, relative energy (ΔE_{tot}) with respect to the lowest energy state, deformation energy of the fragments (E_{def}), binding energy (E_{bind}), and interaction energy (E_{int})

	
D1 $d=3.996$ $\Delta E_{\text{tot}}=0.0$ $E_{\text{def}}=1.7$ $E_{\text{bind}}=-28.3$ $E_{\text{int}}=-30.0$	D2 $d=4.649$ $\Delta E_{\text{tot}}=+0.02$ $E_{\text{def}}=2.3$ $E_{\text{bind}}=-28.2$ $E_{\text{int}}=-30.5$
	
D3 $d=5.445$ $\Delta E_{\text{tot}}=+3.2$ $E_{\text{def}}=0.4$ $E_{\text{bind}}=-25.0$ $E_{\text{int}}=-25.4$	D4 $d=4.749$ $\Delta E_{\text{tot}}=+5.1$ $E_{\text{def}}=0.4$ $E_{\text{bind}}=-23.2$ $E_{\text{int}}=-23.6$

Crystal Structure of the Paraffin Wax

The second point at issue, with the purpose of exploring bee-structure origin, is identification of the wax model that has a vital role in understanding the behavior of the interacting asphaltene-wax systems. As mentioned before, n-paraffin is chosen here as an elementary unit of the macrocrystalline wax. The n-paraffin typically selected is n-C₁₁H₂₄, which is used to form a homologous structural motif of wax components.

The n-paraffin is found as a polymethylene sequence—(CH₂)_n— that regularly packs in layers. The most probable clustering would align the axes of these linear species parallel to each other, to magnify the intermolecular contacts in a wax layer. Based on this principle, the efficient close packing of n-alkanes could be generated by the insertion of protrusions into depressions of the interacting chains (Figure 3-b). The methylene “subcell”, an important concept in the crystallography of wax material, could be constructed by the first two layers. The corresponding layer cell reported in the literature^{61, 62} for the n-undecane paraffin wax is commonly an orthorhombic perpendicular, O_⊥, subcell. In this molecular packing, the carbon-carbon zigzag planes in all alkanes are parallel to each other, except for the molecule located in the body-center site in the unit cell with the plane nearly perpendicular to the others; however, all chains are related by mirror planes (Figure 3-a). The determined dimensions for the aforementioned unit cell of our wax model are shown in Figure 3-c, and are in the range of results predicted by Norman and Mathisen: a_s= 4.89 Å, b_s= 7.22 Å, and γ_s= 90°.⁶²

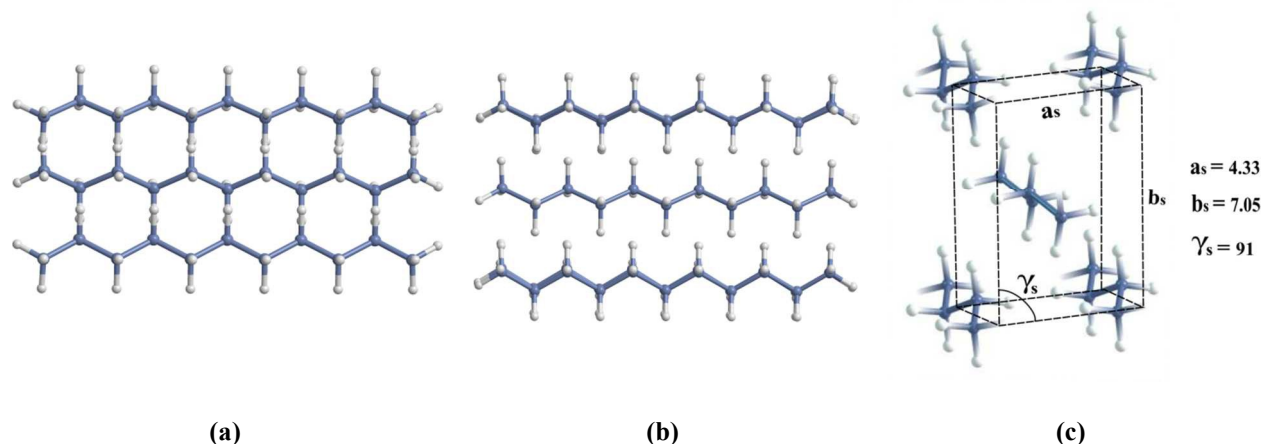


Figure 3. Wax model considered in this study: (a) Close packing of $n\text{-C}_{11}\text{H}_{24}$ molecules (Top-view), (b) Front-view and (c) methylene subcell (O \perp subcell) for the presented packed layer.

The Origin of Bee Structures Based on the Wax-Doped Models

The role of wax crystals in the formation of microstructures, such as bee-like structures, in bitumen has been studied extensively under various viewpoints. The two dominant views, cited in the Introduction section of the paper, are: 1) wax-induced phase separation, in which bee structures are mainly composed of wax crystals, and 2) co-precipitation of wax-asphaltene, in which bee-like features appear in solid-like deposits of wax-asphaltene. In the first hypothesis, bee structures are formed through interactions between non-polar fractions of asphalt binders, including wax crystals, while the nucleation center for wax crystallization can be small amounts of n -paraffin wax. In the second hypothesis, bee structures are attributed to the interaction between polar (such as asphaltene and resin) and non-polar (such as n -paraffin wax) fractions of asphalt binders, and asphaltenes act as nucleation sites for the wax growth and formation of bee structures.

Proponents of each hypothesis present evidence based on asphalt films, imaged by AFM or other imaging techniques, analysis of thermal history, and oxidative aging of samples. As Pauli states,¹⁶ a notable point in these reports is the different interpretations of images that sometimes are very similar.

Despite wide attention to the laboratory investigations of bee-like structures, this issue has not been addressed much from a theoretical viewpoint or with rigorous quantum calculations. So, this paper attempts to use those approaches to evaluate the role of wax and asphaltene in the development of bee-structures.

In this theoretical examination, we studied how a wax crystal influences the interaction between two asphaltene molecules, and whether wax crystals promote self-association of asphaltene sheets. To start, we established models for all required pairs of asphaltene and wax: asphaltene-asphaltene (AA), wax-asphaltene (W-A), and wax-asphaltene-asphaltene (W-AA), as shown in Figure 4. In these structures, we located wax branches parallel to the top face of an asphaltene fragment, in order to have maximum coverage. The optimized geometric structures for stacked models differing in the participating fragments are illustrated in Figure 4. In these models, the asphaltene monomer and dimer have been optimized without imposing any constraints on the systems, as discussed comprehensively above. However, for interacting systems (wax-asphaltene and wax-asphaltene-asphaltene), coordinates of the optimized wax, above the asphaltene, are kept fixed during optimization. Freezing some of the variables provides a way to overcome the practical limitations on studying the large systems. Energy values reported here are in a relative manner, meaning we compared the values for similar species. Accordingly, interaction energies (E_{int}), which include deformation energies of wax and asphaltene, are not reported in the following tables.

Energy information related to the pristine AA and the AA in wax-doped asphaltene complex, in addition to the binding distance between asphaltene sheets, before and after doping are reported in Table 3. Deformation energy of the asphaltene dimer in a wax-doped asphaltene complex relative to that of a pristine dimer (1.4 kcal/mol) is indicative of AA evolution in the presence of wax branches. However, subsequent results reveal that this is not an instructive evolution for an asphaltene dimer. As shown in Table 3, the bonding distance between asphaltene sheets is increased from 3.996 to 4.033 Å in the presence of a wax crystal. This in turn leads to the decrease of binding energy of an AA dimer from -28.3

to -26.9 kcal/mol. Simply stated, an AA dimer is more destabilized in the vicinity of a wax component. These results confirm the unfavorable effect of wax crystals on stacking interaction between unit sheets of asphaltenes.

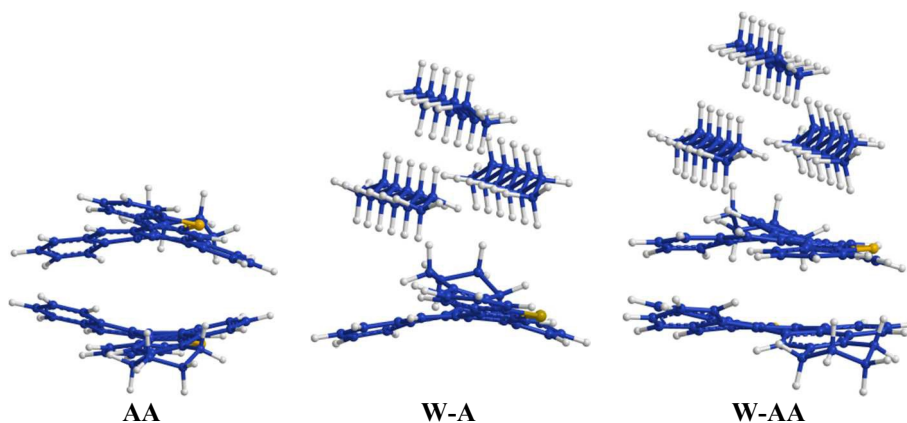


Figure 4. The π -stacked models studied in this paper: asphaltene-asphaltene (AA) dimer, wax-asphaltene (W-A), and wax-asphaltene-asphaltene (W-AA) complex.

Table 3. Comparing asphaltene dimerization in the presence and absence of wax crystal, with all reported energies counterpoise corrected and in kcal/mol. E_{bind} is the binding energy and $E_{\text{def-AA}}$ is the deformation energy of the asphaltene dimer in the presence of a wax crystal.

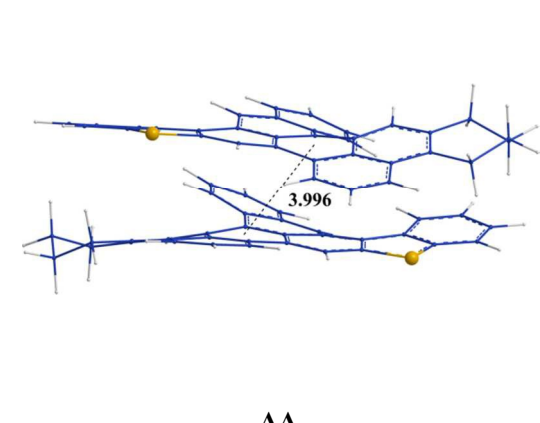
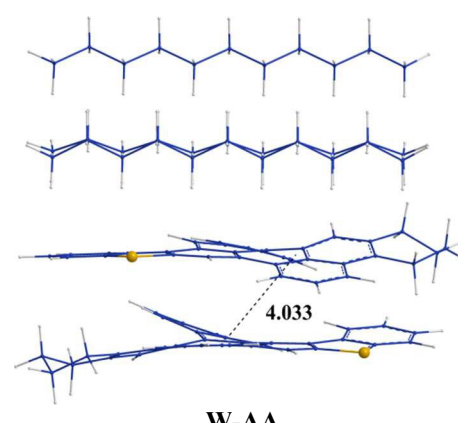
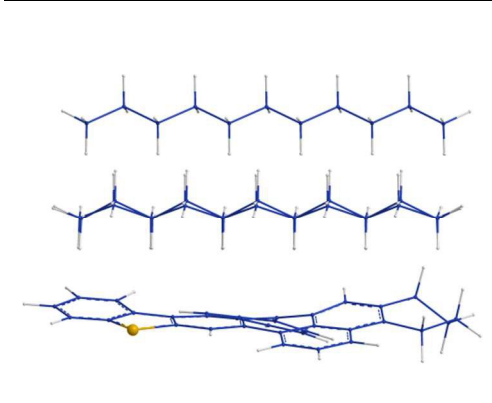
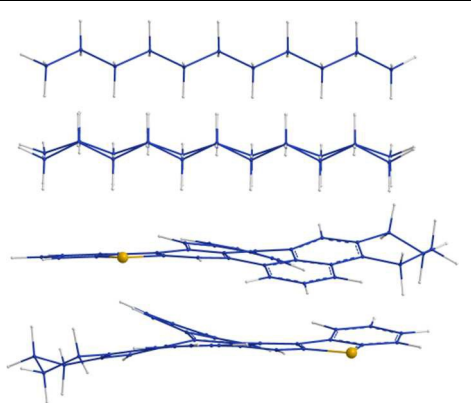
	
AA	W-AA
$E_{\text{bind}} = -28.3$	$E_{\text{bind}} = -26.9$
$E_{\text{def-AA}} = 0.0$	$E_{\text{def-AA}} = +1.4$

Table 4 further supports this finding by comparing the binding energy between fragments of asphaltene monomer and wax component (W-A) with that of asphaltene dimer and wax (W-AA); the effective interaction between wax and a unit sheet of asphaltene is reduced from monomer to dimer. This observation further indicates that by increasing the number of asphaltene sheets, effective interaction between wax phase and non-wax components (asphaltene) is reduced.

Table 4. Comparing optimized stacked models for wax-asphaltene and wax-asphaltene-asphaltene systems: E_{bind} is binding energy, counterpoise corrected and in kcal/mol

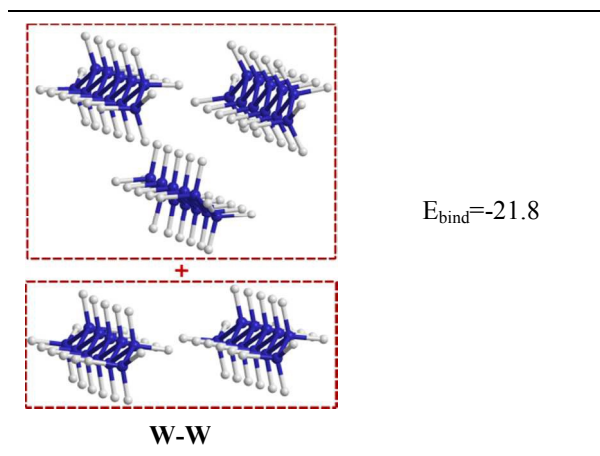
	
W-A	W-AA
$E_{\text{bind}} = -20.9$	$E_{\text{bind}} = -17.6$

Therefore, our calculations reveal that paraffin waxes not only do not reinforce the interaction between the asphaltene unit sheets, paraffin waxes actually destabilize the complex (W-AA) compared to the W-A. This destabilization in interacting systems (asphaltene-asphaltene and also wax-asphaltene) decreases the possibility of the hypothesis that strong interaction between paraffin waxes and non-wax components, such as asphaltene, is responsible for the creation of bee structures.

Wax-Wax Aggregation

To further examine the hypothesis that the bee formation has a direct correlation with the wax crystallization,⁶³ evaluation of the interaction energy for a wax-wax (W-W) complex was performed. To do so, we divided the five n-undecanes ($n\text{-C}_{11}\text{H}_{24}$) into double- and triple-chain groups as interacting wax fragments (marked with red dashed lines in Table 5) and investigated their affinity to aggregate. This fragmentation seems to be quite reasonable, since it is analogous to the design of the alkane chains in the methylene subcell of our wax model (Figure 3). As reported in Table 5, the binding energy for the W-W aggregation is -21.8 kcal/mol, which is 4.2 kcal/mol higher than the corresponding value of a wax-asphaltene (W-AA) complex. This indicates that the interaction between wax crystals (W-W) is thermodynamically more stable than in a wax-doped system of asphaltene (W-AA). This reduces the possibility of co-crystallization of wax and asphaltene, due to the destabilization of asphaltene stacking in the presence of wax, while supporting the hypothesis that the aggregation and crystallization of wax molecules promotes bee formation.

Table 5. Binding energy (counterpoise corrected and in kcal/mol) for interacting wax fragments in a wax-wax aggregation model



Atoms-In-Molecules (AIM) Analysis

To further examine the bond characteristics in our microstructure models, topological analysis of electron density distribution in the intermolecular region was performed. Such characterization is implemented in the AIM theory framework developed by Bader.³⁸ The interaction patterns between fragments are classified according to the properties of critical points (CPs) and bond paths (BPs) in a molecular graph. A bond path is a trajectory of maximum electron density ($\rho(r)$) connecting the nuclei of bonded atoms that indicates all kinds of chemical bonding: strong, weak, closed-shell, and open-shell interactions.⁶⁴ Critical points are electron density extremes in which the gradient of density, $\nabla\rho(r)$, vanishes. They are classified under bond critical points (BCPs), ring critical points (RCPs), and cage critical points (CCPs) by the curvature of the electron density.

The electron density (ρ) and its Laplacian ($\nabla^2\rho$) predicted in bond critical points are important parameters to determine the nature of interactions that correlate with bond strength. Generally, in shared (covalent) bonding, ρ is predominantly greater than 0.20 a.u. and the negative sign of $\nabla^2\rho$ at a bond critical point indicates the accumulation of electric charge in the intermolecular region. On the other hand, in a closed-shell (electrostatic) interaction, density values drop to less than 0.10 a.u., accompanied by depletion of electric charge along the bond (positive value of $\nabla^2\rho$). The electronic energy density,

$H(r) = G(r) + V(r)$, is used to determine the character of interaction, other than using ρ and $\nabla^2\rho$ at the bond critical point. Kinetic energy density (G) is positive and potential energy density (V) is negative,⁶⁵ so the sign of $H(r)$ depends on the relative contributions of potential and kinetic energies at a BCP. Electron-sharing interactions, for which $H(r) < 0$, are dominated by potential energy as a stabilization consequence of the charge accumulation along the bond path. The positive values of $H(r)$ for closed-shell interactions indicate a prevalence of the kinetic energy in the interatomic region.

AIM analysis is appropriate to identify π -stacking and hydrogen bonding interactions through decomposition of multiple contacts between two fragments. The π -stacked systems have been studied by several researchers^{66,67} to find their relation to BCP and CCP data appearing in a contacting zone. Zhikol et al.^{68,69} studied the topology of electron density in the intermolecular region of two interacting benzenes using the AIM method. These authors examined different π -stacking geometries for the benzene dimer and parameterized a correlation equation based on electron density and its Laplacian in the CCPs to predict the potential energy surface; this provided a new evaluation approach for stacking interaction energy.

In the following, we present a brief summary of what has been obtained through topological study of the pristine AA and the AA in wax-doped asphaltene complex as an explanation for the diminished tendency of asphaltene dimerization in the presence of wax crystals.

Asphaltene Dimer

In optimization processing, the parallel D1 structure was identified as the lowest energy state among the possible configurations for asphaltene-asphaltene dimerization. So here, D1 is considered as a model for asphaltene assembly to recognize the nature of interactions and discuss their topological features in the AIM theory framework. A molecular graph of the structure is shown in Figure 5. This topology illustrates all kinds of critical points (BCPs, RCPs, and CCPs) and bond paths between two asphaltenes.

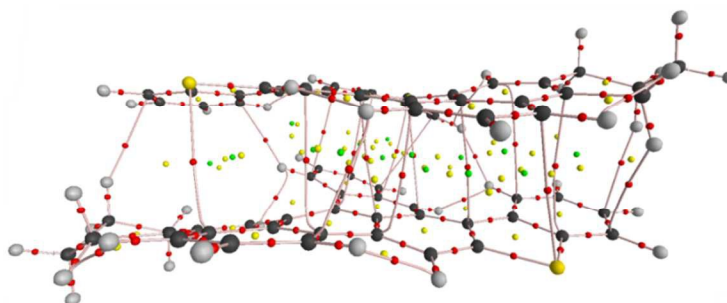


Figure 5. Molecular graph of an asphaltene dimer. The spheres represent the nuclei of atoms: black= C, gray= H, and yellow= S. The dots indicate the position of critical points: red= BCP, yellow= RCP, and green= CCP.

Table 6 lists the principle bond properties at BCPs on the intermolecular paths: electron density, Laplacian of electron density, and electronic energy density. The bond path associated with the binding interactions between asphaltenes exhibits low values for $\rho(r)$ and $\nabla^2\rho(r) > 0$. As the results show, an asphaltene aggregate has 20 BCPs containing twelve C-C (π - π) and five C-H (π -H) CPs with average electron density of 0.0055 and 0.0078 a.u. per bond critical point, respectively. In addition, there are two CPs between the ring and sulfur atoms, each with $\rho = 0.0060$ a.u. All reported electron densities, $\rho(r)$, are an order of magnitude less than 0.10 a.u., so all the corresponding bonds are closed-shell (electrostatic) in nature. Also, all quantities of $\nabla^2\rho(r)$ and $H(r)$ at the BCPs of interacting bond paths are positive, so we can classify them as a closed-shell type of interaction.

In view of the fact that the BCP characteristics are used for qualitative comparison of bond strength, small quantities for electron density at these extreme points indicate weak interactions between two asphaltenes. As reported in the literature,⁷⁰ these kinds of interactions are accountable for the binding between molecules that generates bond paths with the features of closed-shell interactions. Dispersion forces give rise to the accumulation of electron density between fragments and form bond paths through density polarization over nuclei toward each other.⁶⁴ To sum up, it is rational to say that intermolecular interactions in an asphaltene dimer at generic van der Waals distance, $d = 3.394$ Å (the vertical distance between asphaltene sheets), can be attributed to attractive dispersion and repulsive dipole-dipole interactions.

The Zhikol group⁶⁸ used the properties of CCP instead of those of BCP to estimate the stacking interaction in a benzene dimer. Therefore, the other type of critical points, cage CPs, are considered here to visualize the π -stacking nature of interactions. As shown above in Figure 5, there are several CCPs (16 points) in the contacting region. It is worth mentioning that, based on Zhikol's report, the presence of cage critical points is evidence for stacked systems.

Wax-Asphaltene-Asphaltene

In this part, the topological features of an asphaltene dimer isolated from a W-AA complex are considered, to recognize the stabilization of asphaltene stacking in the presence of wax crystals. Table 6 tabulates the properties of critical points between asphaltenes extracted from AIM calculations: $\rho(r)$, $\nabla^2\rho(r)$, and $H(r)$. The trace amount of densities and the positive sign of the Laplacian of density and electronic energy density reveal that the binding interactions are electrostatic in nature.

The number of C-C (π - π) critical points between two asphaltene sheets is nine. Although the average electron density of 0.0058 per C-C critical point is almost equal to the corresponding value in a pristine asphaltene dimer, the reduction in the number of stacking CPs, from 12 to 9, is evidence of the demoting effect of wax crystal on asphaltene assembly.

In addition, the cage critical points (14 points) in the binding region between asphaltenes in this wax-doped model are less than the CCPs in an AA system (16 points), indicating that weakening of π -stack-binding is occurring. This justification is consistent with the conclusion obtained before from the binding energy analysis that the presence of wax could lead to destabilizing the aggregation of asphaltene, making co-crystallization an unlikely event. To further experimentally examine the effect of wax as reflected in asphalt microscopic features and morphology, we used atomic force microscopy (AFM) to study the morphology of various wax-doped asphalt specimens. Accordingly, the aforementioned microscopic features called "bees" were studied at different wax concentrations and humidity conditions.

Table 6. Bond critical point data (in a.u.) from QTAIM analysis for asphaltene-asphaltene and wax-asphaltene-asphaltene dimer

BCP	$\rho(\mathbf{r})$	$\nabla^2\rho(\mathbf{r})$	$H(\mathbf{r})$	BCP	$\rho(\mathbf{r})$	$\nabla^2\rho(\mathbf{r})$	$H(\mathbf{r})$
Asphaltene-Asphaltene							
$H_{(110)}-C_{(29)}$	0.0087	0.0265	0.0012	$C_{(77)}-C_{(24)}$	0.0083	0.0236	0.0010
$H_{(105)}-C_{(28)}$	0.0052	0.0163	0.0009	$C_{(69)}-C_{(11)}$	0.0054	0.0160	0.0007
$C_{(66)}-C_{(31)}$	0.0034	0.0098	0.0005	$C_{(70)}-C_{(12)}$	0.0053	0.0161	0.0008
$C_{(64)}-C_{(26)}$	0.0035	0.0104	0.0005	$C_{(61)}-C_{(13)}$	0.0072	0.0216	0.0010
$C_{(58)}-S_{(27)}$	0.0059	0.0169	0.0008	$H_{(90)}-C_{(3)}$	0.0091	0.0326	0.0018
$C_{(62)}-C_{(16)}$	0.0051	0.0146	0.0007	$C_{(71)}-C_{(4)}$	0.0061	0.0173	0.0008
$H_{(96)}-H_{(42)}$	0.0078	0.0293	0.0016	$C_{(88)}-H_{(39)}$	0.0085	0.0300	0.0016
$C_{(81)}-C_{(21)}$	0.0054	0.0155	0.0007	$S_{(84)}-C_{(6)}$	0.0060	0.0175	0.0009
$C_{(75)}-C_{(19)}$	0.0059	0.0184	0.0009	$C_{(85)}-H_{(53)}$	0.0075	0.0237	0.0012
$C_{(68)}-C_{(17)}$	0.0046	0.0134	0.0006	$C_{(78)}-C_{(22)}$	0.0059	0.0162	0.0007
Wax-Asphaltene-Asphaltene Dimer							
$H_{(53)}-C_{(85)}$	0.0088	0.0280	0.0014	$C_{(3)}-H_{(90)}$	0.0089	0.0311	0.0017
$H_{(38)}-H_{(99)}$	0.0061	0.0226	0.0014	$C_{(14)}-C_{(60)}$	0.0074	0.0215	0.0010
$H_{(39)}-C_{(88)}$	0.0078	0.0273	0.0015	$C_{(15)}-C_{(62)}$	0.0055	0.0159	0.0007
$C_{(7)}-S_{(84)}$	0.0057	0.0163	0.0008	$S_{(27)}-C_{(58)}$	0.0071	0.0205	0.0010
$C_{(24)}-C_{(27)}$	0.0075	0.0212	0.0009	$H_{(42)}-H_{(96)}$	0.0078	0.0296	0.0017
$C_{(22)}-C_{(78)}$	0.0064	0.0178	0.0008	$C_{(31)}-C_{(66)}$	0.0031	0.0092	0.0005
$C_{(4)}-C_{(71)}$	0.0060	0.0171	0.0008	$C_{(28)}-H_{(105)}$	0.0045	0.0145	0.0008
$C_{(12)}-C_{(70)}$	0.0055	0.0166	0.0008	$C_{(29)}-H_{(110)}$	0.0085	0.0260	0.0012
$C_{(19)}-C_{(89)}$	0.0063	0.0197	0.0010	$C_{(26)}-C_{(64)}$	0.0041	0.0118	0.0005
$H_{(37)}-C_{(80)}$	0.0054	0.0166	0.0009				

Evaluation of Bee Formation, Utilizing Atomic Force Microscopy (AFM)

To further examine the effect of wax on bee formation, a study of the surface morphology of asphalt doped with various percentages of wax (1 % to 25 %) was conducted. AFM images of freeze-fractured bitumen surfaces were previously reported exhibiting circular features roughly 10 – 20 μm in diameter.⁷¹ However, moisture from the air could have condensed on the cold fractured surface, and water is known to alter the surface texture of bitumen.⁷² Our own experiments showed that 10 – 40 μm droplets of water condensed on a bitumen surface stored under 100 % humidity at room temperature can significantly

distort the morphology of an asphalt surface.⁷³ Building on our prior work, fracture experiments were performed at room temperature instead of a lower temperature to avoid the possibility of water condensation. Considering that bitumen is a viscoelastic material, brittle fracture can be achieved even at room temperature, provided a high enough strain rate can be applied.

Figure 6 shows AFM images of the native air surface and the bulk fracture surface of undoped, 1% wax-doped, and 3% wax-doped bitumen. The bee structures at the air surface grow in size, amplitude, and wavelength with increasing wax content, consistent with previous studies.⁶³ The fracture surfaces of undoped and doped bitumen reveal “line” features that have not been previously observed, to the best of our knowledge. As highlighted in the magnified inset image of Figure 6d, these lines are small and sparse in undoped bitumen, and the fracture surface is mostly smooth (root mean square roughness, $R_q = 0.5$ nm) except for small asperities that often appear associated with clusters of “lines”. However, the “lines” multiply and lengthen with increasing wax content, and the roughness of the fracture surfaces continues to increase ($R_q = 4.1$ nm for 3 % added wax). Based on this evidence, the aforementioned “lines” are believed to be cross-sections of lamellar paraffin wax crystal inclusions. Figure 7 shows that these inclusions are approximately 10 nm thick for undoped bitumen, in the range of typical thicknesses for paraffin wax lamellae⁷⁴ and consistent with our own previous estimate for the thickness of “bee” structure films.²⁴

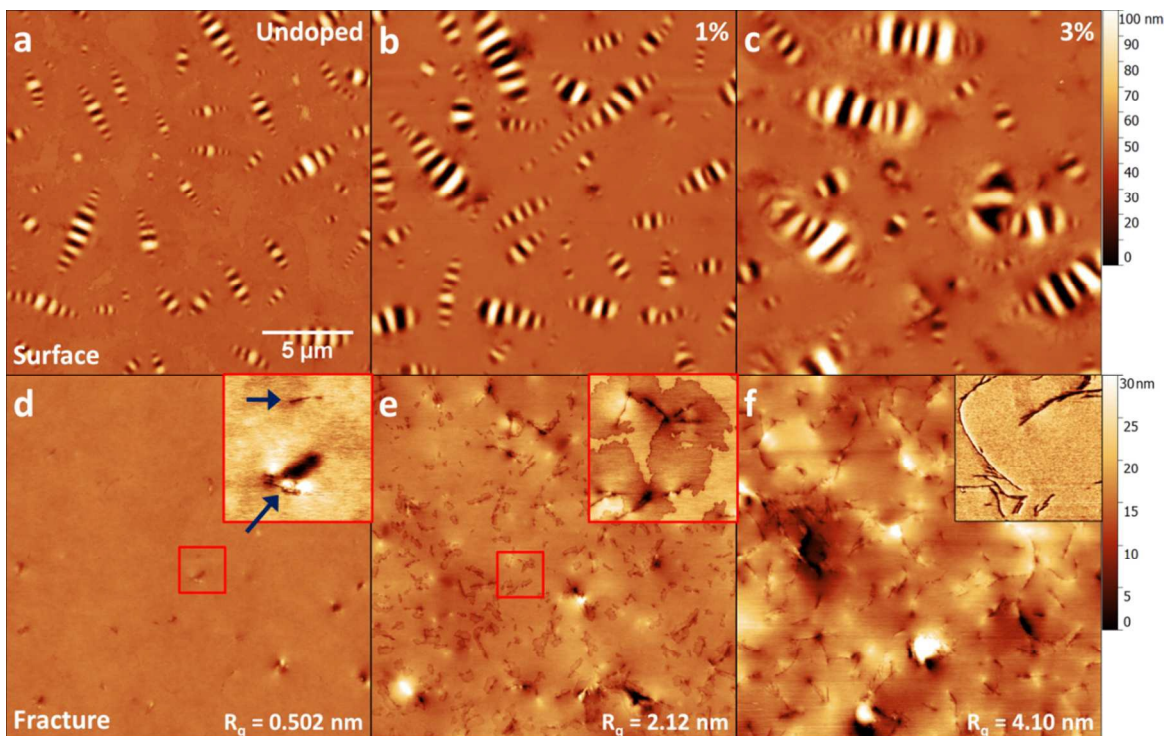


Figure 6. (a-c) AFM images of the surface of bitumen samples doped with paraffin wax (0%, 1%, and 3%, by weight of based asphalt) show an increase in the size of bee structures with the increase of wax content (in Figures a-c, height scale is 100 nm). (d-f) Images of the bulk fracture surface of the same undoped and wax-doped samples, (height scale is 30 nm and all insets are 2.5 μm square areas). (d) The fracture surface of undoped bitumen reveals “line” features (blue arrows) believed to be wax crystals (inset height scale is 4.5 nm). (e) With 1% wax-doping, the “lines” multiply and peri-phase-like regions are observed to grow around the “lines” during imaging (inset height scale is 10 nm). (f) At 3% wax-doping, large “lines” are clearly visible and roughness (R_q) increases (inset is a phase image).

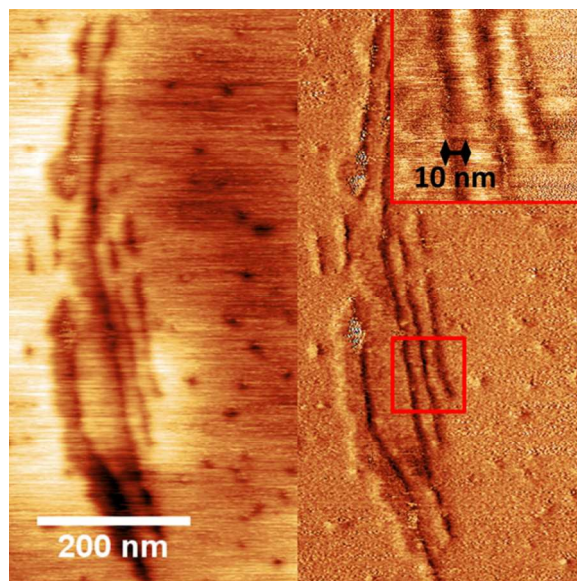


Figure 7. AFM topography (left, height scale 5 nm) and phase (right) images of the fracture surface of undoped bitumen show that the “lines” are approximately 10 nm thick.

Figure 6e appears to show peri-phase-like areas beginning to grow around these inclusions in 1% wax-doped bitumen. These peri-phase-like areas grow larger during imaging (Figure 6e inset), sometimes nucleating on one side of an inclusion first before expanding to envelop it. Figure 8 demonstrates that the same process of peri-phase growth occurs over a longer time period around the visible inclusions on the fracture surface of undoped bitumen. After one week (Figure 8a), peri-phase-like areas have nucleated around nearly every inclusion similar to what was observed in Figure 6. After two weeks (Figure 8b), these peri-phase-like areas have grown into diamond-shaped features reminiscent of previously reported polyethylene single crystals.⁷⁵ While every inclusion seeds a “diamond,” they are not required for “diamond” formation, since a handful of “diamonds” appear not to contain an inclusion. After three weeks (Figure 8c), small catana-phase areas appear, indicating that these “diamonds” are indeed precursors to bee structures.

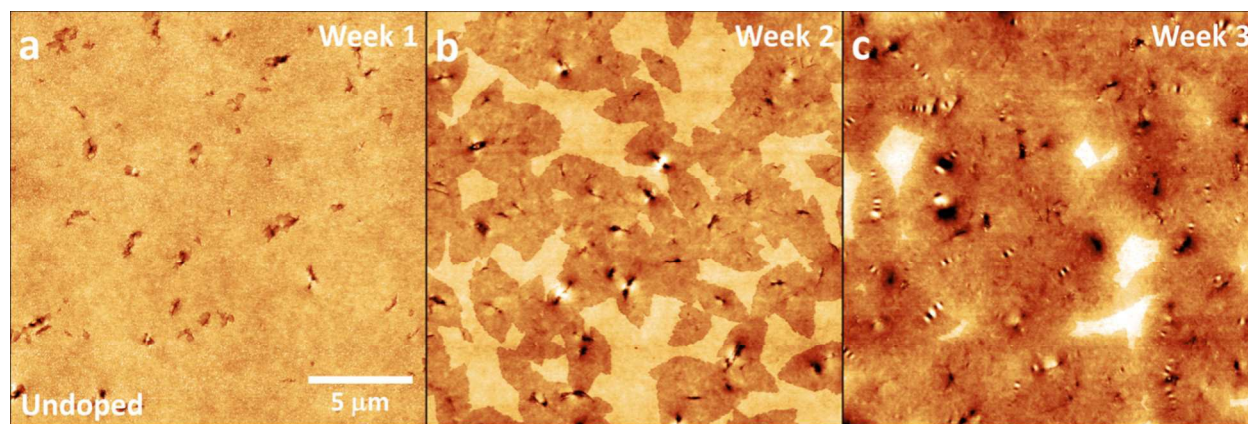


Figure 8. AFM height images of the undoped bitumen fracture surface and its evolution over 3 weeks of storage under ambient conditions (22 °C, 50% humidity). Height scale is 10 nm.

Figure 9 shows that with 10% added wax, the bee structures on the surface disappear and are replaced by a lamellar, terraced topography common to paraffin wax. The thickness of the lamellae here is 3 – 5 nm. The difference between this measurement and Figure 7 may be due to either a difference between lateral resolutions versus depth resolution in AFM or a difference between the thicknesses of

lamellar wax crystals in the bulk compared to surface. The fracture surface of 10% wax-doped bitumen is significantly rougher ($R_q = 340$ nm), revealing in a few locations what are believed to be the flat faces of the lamellar wax inclusions (Figure 9b, yellow arrows). In the most extreme case, the fracture surface of a 25% wax-doped bitumen sample shows lamellar terraces suggesting that the cracks propagated along the wax inclusions almost exclusively.

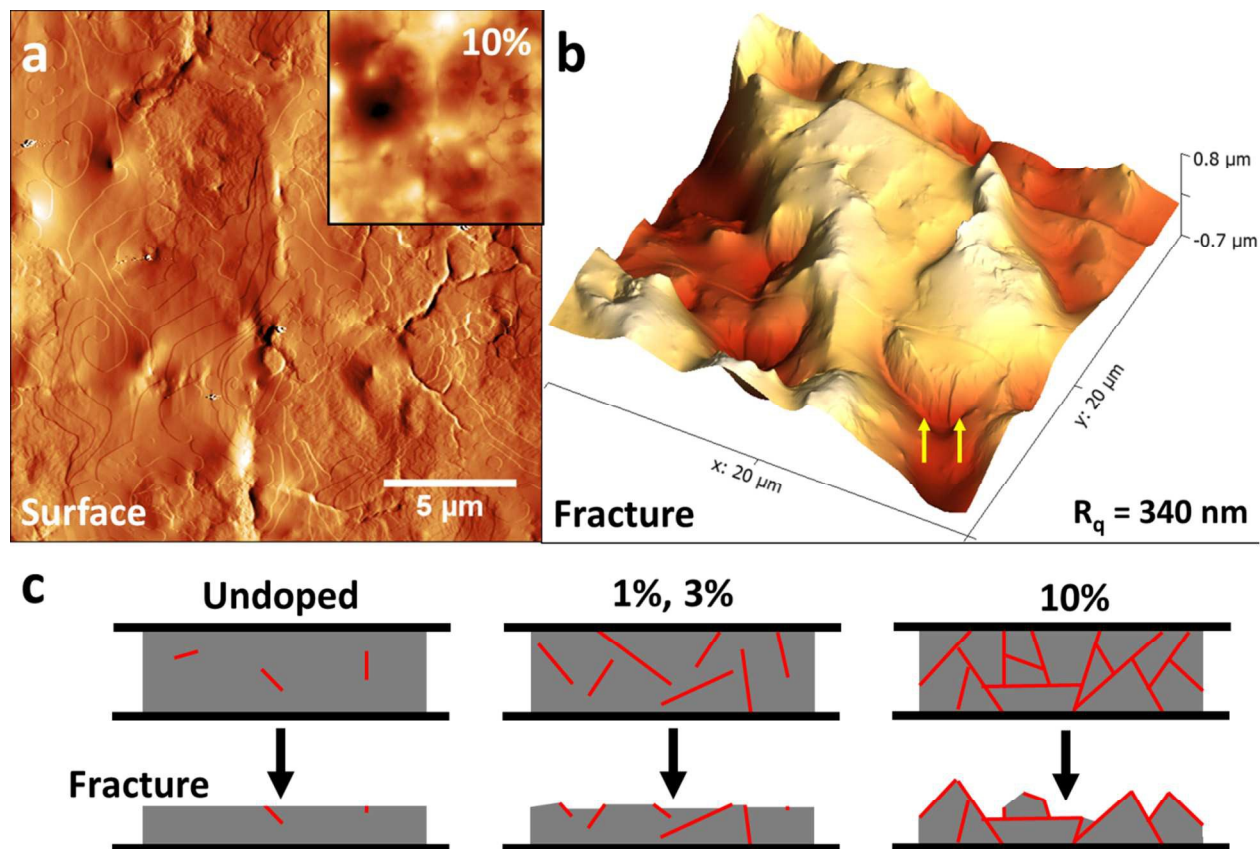


Figure 9. (a) AFM amplitude image of the surface of 10% wax-doped bitumen shows no bee structures but lamellar terraces of paraffin wax (inset shows the corresponding height image with 320 nm height scale). (b) AFM 3-D image of the fracture surface of 10% wax-doped bitumen. Arrows highlight a “cliff” that exposes what is thought to be the flat faces of embedded paraffin wax crystals. (c) Schematic illustration of how increasing wax content might form a percolating network of wax crystals (red) along which cracks propagate, resulting in a rougher fracture surface.

We hypothesize that the distribution of the wax constituent in bitumen is partly governed by its “solubility limit” in the bitumen resin, which defines the concentration of wax that can be mixed at the molecular level with the other bitumen constituents at chemical equilibrium and not precipitate out as an

inclusion or separate phase. At low concentrations, all of the contained wax can be homogeneously mixed or “dissolved” in the resin components. As the wax content increases, it will get dissolved until a solubility limit is reached. Above the solubility limit, no additional wax can be mixed in with the resin, and the excess wax separates and crystallizes out as heterogeneous inclusions. Note that material behavior at a surface or interface can be different, so separation at the surface may occur at lower wax concentrations than in the bulk.

The native PG 64-22 bitumen may already be close to wax-saturated, so even a small amount of added wax crystallizes out readily, as observed by AFM imaging. These wax inclusions appear to be lamellar sheets roughly 10 nm thick, similar in structure and composition to what was documented to be responsible for the bee structures.²⁴ Indeed, Figure 8 demonstrates how the bees often nucleate off the inclusions, an effect that can be described as “seeded” or heterogeneous nucleation of crystal growth. However, it should be noted that “unseeded” or homogeneous nucleation is also possible, so exposed inclusions at the surface are not required for bee formation, even though heterogeneous nucleation is typically more prevalent. The DFT results suggest that these crystals are pure wax and unlikely to be co-crystallized with asphaltene, which is consistent with the equilibrium phase behavior of most materials. The mixing of two solid components often leads to melting point depression such as in a eutectic mixture, and the solid phases only exist for relatively pure compositions.^{76, 77}

The wax inclusions appear to act as weak points in the bitumen fracture experiments. Figure 9c offers a schematic illustration of how the bitumen fracture behavior may change with increasing wax content. The propagating crack may follow the contours of an inclusion, and with increasing wax content, the inclusion crystals grow, resulting in a rougher fracture surface. With 10% or more added wax, the lamellar inclusions are large and frequent enough to connect together in a continuous network. At that point, a propagating crack can almost exclusively follow the inclusions, resulting in a dramatically rougher fracture surface. The fracture weakness of these inclusions might stem from two effects: low fracture strength of pure paraffin wax or poor adhesion between wax inclusions and the bitumen

components. The DFT results presented above lend credence to the latter possibility, showing that the interaction between crystallized wax and the asphaltene and other polar constituents may be relatively weak or unfavorable.

Another consequence of the DFT results is that the bitumen may become softer with increasing wax content. Table 7 lists the predominant wavelengths of the bee structures as measured from AFM images using fast Fourier transform (FFT) analysis as previously described.²⁴ The reported error is double the standard error of the mean. The calculated values corroborate the impression given by the AFM images that the bee wavelength increases with increasing wax content. Based on the model of the bee structures as stiff, rippled thin films on a soft resin substrate, the wavelength λ_o of the ripples is dependent on the thickness of the film h and the plane-strain moduli of the film \bar{E}_f and substrate \bar{E}_s as shown in Equation 3 below:⁷⁸

$$\lambda_o = 2\pi h \left(\frac{\bar{E}_f}{3\bar{E}_s} \right)^{1/3} \quad (3)$$

If the molecular composition and crystal structure of the bee film does not change, then \bar{E}_f should be constant. An increase in h is likely responsible for much of the increase in λ_o , as multiple paraffin lamellae may stack together with increasing paraffin concentration. Based on thermodynamics principles, \bar{E}_s should not change with increasing amounts of added wax, because above the solubility limit, any additional wax should crystallize out as inclusions, and the composition of the substrate bitumen matrix should not change. However, this theory describes thermodynamic equilibrium behavior and does not consider the possibility that the resin composition may be supersaturated with wax and not be at equilibrium. It is conceivable then that some of the increase in λ_o reflects a decrease in \bar{E}_s due to added wax molecules that both dilute and weaken the otherwise strong interactions between polar and aromatic constituents in the bitumen, in accordance with the DFT results. Empirically, it was observed that when the wax content increased, lower forces were required to bring the bitumen film to cohesive fracture; it was further noticed that only with the undoped bitumen was there a consistent danger of shattering the

glass slides when attempting to split the sandwiched bitumen specimen. If wax supersaturation is possible, then more wax will eventually separate from the mixture over time, leading to stiffening of the resin matrix with age. To test this hypothesis, further investigation of the material and mechanical properties of wax-doped bitumen are ongoing.

Table 7. Predominant wavelength of the bee structures from FFT analysis of AFM images

Wax doping (wt%)	Wavelength (nm)	Images analyzed
0	651 ± 26	5
1	867 ± 12	3
3	1038 ± 13	3

CONCLUSION

There have been several experimental analyses to characterize the microstructure features in asphalt called bees. In addition, recent studies have established a relation between bee sizes and rheological properties of asphalt, indicating bee length can have a moderating effect on the relationship between viscosity and stiffness of asphalt binder, and that binders with larger bees typically show higher stress amplification due to tensile deformation, making asphalt more prone to damage. Although the impact of bees on asphalt properties has been documented, disagreement remains about the bees' nature and origin, as well as their impact on asphalt oxidation. While several studies refer to the bees as solely surface features, some others consider them to be bulk microcrystalline components that form due to co-precipitation of wax and asphaltene molecules.

Accordingly, it is essential to understand the interplay of asphalt components (mainly asphaltene and wax) in the formation of bees, using a rigorous theoretical approach. Therefore, this study has investigated the effect of paraffin wax on the dimerization of asphaltenes, as a probable cause of aggregation and co-precipitation to form bee-structures. With this aim, the stacking of asphaltene-asphaltene in the presence and absence of wax fragments was studied. Moreover, the interaction of wax

and asphaltene was examined to understand the role of n-paraffin wax in the formation of bee-like microstructures.

To study the role of n-paraffin wax, the geometries of the monomer fragments, asphaltene and wax, and their stacking systems (asphaltene-asphaltene, wax-asphaltene, and wax-asphaltene-asphaltene) were optimized at the B97-D/6-31G* level of theory. The thermodynamic stability of aggregations was examined by calculating the binding energy, E_{bind} . The results obtained at this level of computation show that T-shaped conformation is not favored for an asphaltene dimer, and that the dimer of asphaltene falls into a parallel arrangement. Therefore, the most stable configuration (D1 in Table 2) was selected among the four lowest-energy parallel structures, which were different in the relative position of sulfur atoms in asphaltenes. This lowest-energy structure was the target structure for our investigations in subsequent steps. Energy information and electronic structure analysis, using an AIM approach, were two criteria used to evaluate the strength of interactions between asphaltene sheets in the presence and absence of wax crystal.

Binding energy and deformation energy values show that the n-paraffin wax imposes deformation on the asphaltene dimer in the wax-doped model; however, this deformation is not in favor of asphaltene dimerization. This observation is supported by the comparison of binding energies for isolated dimers in a wax-asphaltene-asphaltene complex and in a pristine asphaltene-asphaltene system. This observation is also consistent with the AIM analysis finding of a decrement of critical points between asphaltenes, indicating the negative effect of a wax component on asphaltene dimerization. Further study of binding energy for a wax-wax complex showed that the interaction between wax crystals is thermodynamically more stable (by 4.2 kcal/mol) than in a wax-doped system of asphaltene. This, in turn, supports the hypothesis that the aggregation and crystallization of wax molecules are likely to promote bee formation. Moreover, the co-crystallization of wax and asphaltene was found not to be thermodynamically favorable; rather, the presence of wax destabilized the assembly of asphaltene molecules, causing a reduction of aggregation.

The experimental analysis performed using atomic force microscopy (AFM) on a wax-doped asphalt complex further showed the appearance of coarser surfaces as the percentages of wax increased from 1% to 3%. A fractured surface in non-wax bitumen was found to be quite smooth (with root mean square roughness of $R_q = 0.5$ nm). However, the fracture surfaces continued to become rougher as the wax content increased ($R_q = 4.1$ nm at 3 % wax, and $R_q = 340$ nm at 10% wax). Analysis of AFM images further showed as the wax content increases so does the bee wavelength; this was in agreement with DFT calculation results indicating that the interaction between wax molecules and those of asphaltene are relatively weak, and that wax-wax aggregation is more favorable than wax-asphaltene co-aggregation. Therefore, the presence of wax could possibly reduce overall stiffness of the matrix and thus reduce \bar{E}_S ; this along with an increased thickness of the film due to a stacked wax lamellar structure could be the cause of the observed increase in bee wavelength from 651 to 1038 nm when the non-wax bitumen was doped with 3% wax.

Bee size has been shown to have a moderating effect on the relationship between viscosity and stiffness, and on the level of stress amplification due to constant deformation in asphalt.^{25, 26} Therefore, understanding bee structures and their evolution in wax-doped asphalt could provide insight on asphalt performance characteristics. Further study is ongoing to examine thermal and rheological properties of wax-doped asphalt after long-term aging to examine scenarios pertaining to supersaturation of wax-doped bitumen and its time-dependent stiffening effect due to phase separation.

ACKNOWLEDGMENT

The authors would like to acknowledge the support provided by the National Science Foundation, Award No: 1150695. The contents of this paper reflect the view of the authors, who are responsible for the facts and the accuracy of the data presented.

REFERENCES

1. *Paving Asphalt Price Index*. http://www.dot.ca.gov/hq/esc/oe/asphalt_index/astable.html, accessed June 1, 2015.

2. *The Bureau of Transportation Statistics (BTS)*, <http://www.bts.gov>, last visited January, 2013.
3. *National Asphalt Pavement Association*, <http://www.hotmix.org>, Accessed 22 April 2013.
4. D. Lesueur, J. F. Gerard, P. Claudy, J. M. Letoffe, J. P. Planche and D. Martin, *Journal of Rheology (1978-present)*, 1996, **40**, 813-836.
5. L. Loeber, G. Muller, J. Morel and O. Sutton, *Fuel*, 1998, **77**, 1443-1450.
6. J. F. MASSON, V. Leblond, J. Margeson and S. BUNDALO-PERC, *Journal of microscopy*, 2007, **227**, 191-202.
7. D. Lesueur, *Advances in colloid and interface science*, 2009, **145**, 42-82.
8. J. F. MASSON, V. Leblond and J. Margeson, *Journal of Microscopy*, 2006, **221**, 17-29.
9. E. Sourty, A. Tamminga, M. Michels, W. P. VELLINGA and H. Meijer, *Journal of microscopy*, 2011, **241**, 132-146.
10. L. Loeber, O. Sutton, J. Morel, J. M. Valleton and G. Muller, *Journal of Microscopy*, 1996, **182**, 32-39.
11. S.-p. Wu, L. Pang, L.-t. Mo, Y.-c. Chen and G.-j. Zhu, *Construction and Building Materials*, 2009, **23**, 1005-1010.
12. A. Pauli, J. Branthaver, R. Robertson, W. Grimes and C. Eggleston, *Preprints-American Chemical Society. Division of Petroleum Chemistry*, 2001, **46**, 104-110.
13. A. Jäger, R. Lackner, C. Eisenmenger-Sittner and R. Blab, *Road Materials and Pavement Design*, 2004, **5**, 9-24.
14. M. De Moraes, R. Pereira, R. Simão and L. Leite, *Journal of Microscopy*, 2010, **239**, 46-53.
15. A. Schmets, N. Kringos, T. Pauli, P. Redelius and T. Scarpas, *International Journal of Pavement Engineering*, 2010, **11**, 555-563.
16. A. Pauli, R. Grimes, A. Beemer, T. Turner and J. Branthaver, *International Journal of Pavement Engineering*, 2011, **12**, 291-309.
17. H. Soenen, J. Besamusca, H. R. Fischer, L. D. Poulidakos, J.-P. Planche, P. K. Das, N. Kringos, J. R. Grenfell, X. Lu and E. Chailleux, *Materials and structures*, 2014, **47**, 1205-1220.
18. H. R. Fischer, E. Dillingh and C. Hermse, *Road Materials and Pavement Design*, 2014, **15**, 1-15.
19. M. d. C. García and L. Carbognani, *Energy & Fuels*, 2001, **15**, 1021-1027.
20. M. d. C. García, *Energy & fuels*, 2000, **14**, 1043-1048.
21. S. Nahar, A. Schmets, A. Scarpas and G. Schitter, *European Polymer Journal*, 2013, **49**, 1964-1974.
22. R. G. Allen, D. N. Little, A. Bhasin and C. J. Glover, *International Journal of Pavement Engineering*, 2014, **15**, 9-22.
23. R. G. Allen, D. N. Little and A. Bhasin, *Journal of Materials in Civil Engineering*, 2012, **24**, 1317-1327.
24. A. M. Hung and E. H. Fini, *RSC Advances*, 2015, (accepted with revision).
25. E. Fini, D. J. Oldham and a. M. Parast, *The Peterson Asphalt Research Conference, Laramie, Wyoming* 2015.
26. R. Jahangir, D. Little and A. Bhasin, *International Journal of Pavement Engineering*, 2015, **16**, 337-349.
27. M. J. Frisch, G. W. Trucks, H. B. Schlegel and e. al., *revision A.1, Gaussian, Inc., Wallingford CT*, 2009.
28. J. Seponer, J. Leszczynski and P. Hobza, *Journal of computational chemistry*, 1996, **17**, 841-850.
29. S. Grimme, *Journal of computational chemistry*, 2006, **27**, 1787-1799.
30. S. Grimme, J. Antony, S. Ehrlich and H. Krieg, *The Journal of chemical physics*, 2010, **132**, 154104.
31. A. D. Becke, *The Journal of chemical physics*, 1997, **107**, 8554-8560.
32. M. Witko and K. Hermann, *Applied Catalysis A: General*, 1998, **172**, 85-95.

33. M.-L. Bocquet, P. Sautet, J. Cerda, C. I. Carlisle, M. J. Webb and D. A. King, *Journal of the American Chemical Society*, 2003, **125**, 3119-3125.
34. W. Gao, M. Zhao and Q. Jiang, *The Journal of Physical Chemistry C*, 2007, **111**, 4042-4046.
35. W. Liu, J. Lian and Q. Jiang, *The Journal of Physical Chemistry C*, 2007, **111**, 18189-18194.
36. G.-J. Kang, Z.-X. Chen and Z. Li, *The Journal of chemical physics*, 2009, **131**, 034710-034710.
37. S. F. Boys and F. d. Bernardi, *Molecular Physics*, 1970, **19**, 553-566.
38. R. F. W. Bader, *Clarendon: Oxford, UK*, 1990, 188-250.
39. R. Bader.
40. D. Borton, D. S. Pinkston, M. R. Hurt, X. Tan, K. Azyat, A. Scherer, R. Tykwinski, M. Gray, K. Qian and H. I. Kenttämäa, *Energy & Fuels*, 2010, **24**, 5548-5559.
41. H. Sabbah, A. L. Morrow, A. E. Pomerantz, O. C. Mullins, X. Tan, M. R. Gray, K. Azyat, R. R. Tykwinski and R. N. Zare, *Energy & Fuels*, 2010, **24**, 3589-3594.
42. H. Sabbah, A. L. Morrow, A. E. Pomerantz and R. N. Zare, *Energy & Fuels*, 2011, **25**, 1597-1604.
43. J. P. Dickie and T. F. Yen, *Analytical chemistry*, 1967, **39**, 1847-1852.
44. D. D. Li and M. L. Greenfield, *Fuel*, 2014, **115**, 347-356.
45. D. D. Li and M. L. Greenfield, *Energy & Fuels*, 2011, **25**, 3698-3705.
46. O. C. Mullins, *Energy & Fuels*, 2010, **24**, 2179-2207.
47. L. Zhang and M. L. Greenfield, *Energy & fuels*, 2007, **21**, 1102-1111.
48. F. J. Martín-Martínez, E. H. Fini and M. J. Buehler, *RSC Advances*, 2015, **5**, 753-759.
49. R. D. Dennington, T. A. Keith and J. M. Millam, *Gaussian Inc*, 2008.
50. L. J. Lowden and D. Chandler, *The Journal of Chemical Physics*, 1974, **61**, 5228-5241.
51. A. Narten, *The Journal of Chemical Physics*, 1977, **67**, 2102-2108.
52. M. Alonso, T. Woller, F. J. Martín-Martínez, J. Contreras-García, P. Geerlings and F. De Proft, *Chemistry-A European Journal*, 2014, **20**, 4931-4941.
53. D. Evans and R. Watts, *Molecular Physics*, 1976, **32**, 93-100.
54. J. Rodríguez, J. Sánchez-Marín, F. Torrens and F. Ruetze, *Journal of Molecular Structure: THEOCHEM*, 1992, **254**, 429-441.
55. J. Pacheco-Sánchez, F. Alvarez-Ramirez and J. Martínez-Magadán, *Energy & fuels*, 2004, **18**, 1676-1686.
56. J. Pacheco-Sánchez, I. Zaragoza and J. Martínez-Magadán, *Energy & fuels*, 2003, **17**, 1346-1355.
57. M. Sedghi, L. Goual, W. Welch and J. Kubelka, *The Journal of Physical Chemistry B*, 2013, **117**, 5765-5776.
58. F. Alvarez-Ramírez and Y. Ruiz-Morales, *Energy & Fuels*, 2013, **27**, 1791-1808.
59. C. A. Hunter, K. R. Lawson, J. Perkins and C. J. Urch, *Journal of the Chemical Society, Perkin Transactions 2*, 2001, 651-669.
60. C. A. Hunter and J. K. Sanders, *Journal of the American Chemical Society*, 1990, **112**, 5525-5534.
61. S. Abrahamsson, B. Dahlen, H. Löfgren and I. Pascher, *Progress in the Chemistry of Fats and other Lipids*, 1978, **16**, 125-143.
62. N. Norman and H. Mathisen *Acta Chemica Scandinavica*, 1972, **26**, 3913-3916.
63. T. Pauli, W. Grimes, J. Beiswenger and A. J. Schmets, *Journal of Materials in Civil Engineering*, 2015, C4014001.
64. R. F. Bader, *The Journal of Physical Chemistry A*, 1998, **102**, 7314-7323.
65. D. Cremer and E. Kraka, *Angewandte Chemie International Edition in English*, 1984, **23**, 627-628.
66. M. P. Waller, A. Robertazzi, J. A. Platts, D. E. Hibbs and P. A. Williams, *Journal of computational chemistry*, 2006, **27**, 491-504.
67. C. F. Matta, N. Castillo and R. J. Boyd, *The Journal of Physical Chemistry B*, 2006, **110**, 563-578.

68. O. A. Zhikol, O. V. Shishkin, K. A. Lyssenko and J. Leszczynski, *The Journal of chemical physics*, 2005, **122**, 144104.
69. O. A. Zhikol and O. V. Shishkin, *International Journal of Quantum Chemistry*, 2012, **112**, 3008-3017.
70. R. G. Bone and R. F. Bader, *The Journal of Physical Chemistry*, 1996, **100**, 10892-10911.
71. H. R. Fischer and B. Dillingh, *Road Materials and Pavement Design*, 2015, **16**, 31-45.
72. S. dos Santos, M. N. Partl and L. D. Poulikakos, *Construction and Building Materials*, 2014, **71**, 618-627.
73. A. M. Hung, A. Goodwin and E. H. Fini, *Transportation Research Record*, 2015, (accepted).
74. M. Kané, M. Djabourov, J.-L. Volle, J.-P. Lechaire and G. Frebourg, *Fuel*, 2003, **82**, 127-135.
75. A. Toda, M. Okamura, M. Hikosaka and Y. Nakagawa, *Polymer*, 2005, **46**, 8708-8716.
76. C. Kittel and H. Kroemer, Freeman, 1980.
77. S. Prasad Das, *Cambridge University Press*, 2011, ISBN-13:9780521858397, 2011, **1**.
78. H. Jiang, D.-Y. Khang, J. Song, Y. Sun, Y. Huang and J. A. Rogers, *Proceedings of the National Academy of Sciences*, 2007, **104**, 15607-15612.